RESEARCH ARTICLE

NANO · MICRO small
www.small-journal.com

Enhanced Conductivity in Conjugated Microporous Polymers via Integrating of Carbon Nanotubes for Ultrasensitive NO_2 Chemiresistive Sensor

Weisi He, Qian-Wen Li, Sijie Chen, He Liu, Zhonghua Cheng, Shuang Li, Wei Lyu, Gang Xu,* Yong-Jun Chen,* and Yaozu Liao**

Conjugated microporous polymers (CMPs) present high promise for chemiresistive gas sensing owing to their inherent porosities, high surface areas, and tunable semiconducting properties. However, the poor conductivity hinders their widespread application in chemiresistive sensing. In this work, three typical CMPs (PSATA, PSATB, and PSATT) are synthesized and their chemiresistive gas sensing performance is investigated for the first time. To further improve performance, PSATT are modified on the surface of amino-functionalized multi-walled carbon nanotubes (NH_2-MWCNTs) to improve the conductivity. As a result, the obtained material, PSATT-7NC exhibited a high sensitivity of 9766% toward 4 ppm NO_2, which is 2.5 times higher than that of pristine PSATT. It also demonstrated remarkable selectivity and excellent long-term stability. Furthermore, the lowest limit of detection (0.79 ppb) among all polymers-based sensors is achieved at a low operating temperature of 100 °C. This work provides a valuable strategy into the development of a new material platform for advancing high-performance gas sensing applications.

1. Introduction

As the fundamental component of olfactory sensing, gas sensors have extensive potential applications in environmental monitoring, public safety, healthcare, food safety, military aerospace, and other fields.[1–4] Compared with other gas detection, chemiresistive gas sensor converts the type and concentration of gas into resistance change as a readout signal with the advantages, including simplified device design, low cost, high sensitivity, and long life.[5–7] The most used chemiresistive sensing materials employing metal oxide semiconductors (MOS) have inherent shortcomings, such as poor selectivity, high operating temperatures, and high power consumption.[8,9] All of these serve to limit the practical application and industrial development of gas sensors. Thus, there is an urgent requirement to explore alternative gas sensing materials that can offer high sensitivity and operate at a relatively low temperature to cut down on energy usage, all without compromising on sensitivity.

Porous organic polymers (POPs) are a class of porous networks constructed from organic building unit by strong covalent bonds.[10,11] Due to their diverse structures, high stability, and large surface area, POPs hold great promise in many applications, such as gas storage, catalysis, sensing, energy storage, and conversion.[12–15] Currently, covalent organic frameworks (COFs) and covalent triazine frameworks (CTFs), act as POPs, are used in chemiresistive gas sensors. Compared to COFs and CTFs, conjugated microporous polymers (CMPs), another type of POPs, offer a simpler synthesis method that is not constrained by crystallization or specific reaction conditions. Additionally, CMPs not only possess the characteristics of POPs, but also exhibit unique semiconducting properties due to their large ring-conjugated framework structure.[16,17] This makes CMPs highly promising for chemiresistive gas sensing materials. Although optical chemical sensors are fabricated,[10,18,19] CMPs have not yet been utilized in the realm of chemiresistive gas sensing. This is mainly attributed to the poor processability and low conductivity of CMPs, which hinders the effective electron transfer in chemiresistive gas sensing.

W. He, S. Chen, H. Liu, Z. Cheng, W. Lyu, Y. Liao
State Key Laboratory for Modification of Chemical Fibers and Polymer Materials
College of Materials Science and Engineering
Donghua University
Shanghai 201620, China
E-mail: fduchengzh@163.com; yzliao@dhu.edu.cn

Q.-W. Li, G. Xu, Y.-J. Chen
State Key Laboratory of Structural Chemistry
Fujian Provincial Key Laboratory of Materials and Techniques toward Hydrogen Energy
Fujian Institute of Research on the Structure of Matter
the Chinese Academy of Sciences
Fuzhou, Fujian 350002, P. R. China
E-mail: gxu@fjirsm.ac.cn; chenyongjun@fjirsm.ac.cn

S. Li
College of Polymer Science and Engineering
State Key Laboratory of Polymer Materials Engineering
Sichuan University
Chengdu 610065, China

G. Xu
University of Chinese Academy of Sciences (UCAS)
Beijing 100049, P. R. China

The ORCID identification number(s) for the author(s) of this article can be found under https://doi.org/10.1002/smll.202407880

DOI: 10.1002/smll.202407880

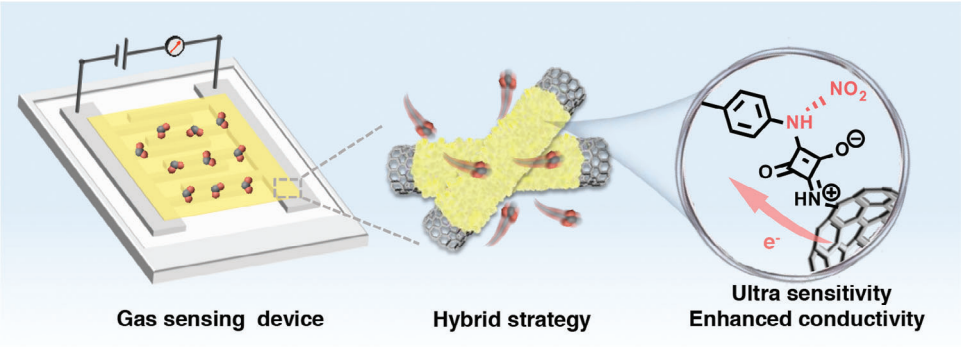

Scheme 1. Scheme showing the design principle of CMPs for the detection of NO_2 with enhanced conductivity and improved sensitivity.

To obtain high-performance sensing materials, it is necessary to enhance the conductivity of CMPs. The hybrid strategy of CMPs and amino-functionalized multi-walled carbon nanotubes (NH_2-MWCNTs) might be a good choice for improving conductivity to bring excellent CMPs-based chemiresistive gas sensing. This is due to: 1) The surface amino groups of NH_2-MWCNTs provide the strong forces for hybridizing CMPs, 2) Large delocalization system and interlayer π–π interactions of CMPs lead to efficient electrons transport between complexes,[20–22] and 3) High conductivity of NH_2-MWCNTs serves as electrons transfer channels for CMPs to bring improved conductivity and sensitivity. In the CMPs and NH_2-MWCNTs integrated system, it can be assumed that hybrid materials with high surface area and conductivity ensure effective gas adsorption and electron transfer to achieve high-performance chemiresistive gas sensing. In addition, most conjugated polymers adsorb gas molecules primarily through dispersive forces or dipole-dipole interactions, which are insufficient for efficient charge transfer between the material and the gas molecules. Constructing stronger interactions, such as hydrogen bonds or ionic dipoles with the target gas molecules is a promising approach. Lu et al.[23] prepared a linear conjugation polymer, para-polyphenylsquaraine (*p*-PPS), with high sensitivity to NO_2 via a reaction between squaric acid and o-phenyldiamines under reflux conditions. It has been demonstrated that squaric acid, with its unique zwitterionic resonance structure, provides a zigzagged skeleton and extends the π-conjugation, which is beneficial to enhance charge transfer and improve sensing performance. Subsequently, He et al.[24] constructed a squaric acid-based COFs (SA-TAPB) with high selectivity for NO_2 through the solvothermal condensation between squaric acid and 1,3,5-tris(4-aminophenyl) benzene in o-dichlorobenzene catalyzed by acetic acid. The results indicate that hydrogen bonding and ionic dipole interactions between SA-TAPB and NO_2 facilitate the reversible adsorption and desorption of NO_2, thereby improving sensing performance. Therefore, squaric acid-based CMPs exhibit potential as effective sensing materials, as their large delocalization system and the π-π interaction effectively enhance the charge transfer, while their ionic dipole and hydrogen bonding interactions with NO_2 ensure reversible adsorption and desorption of gas molecules.

As a proof-of-concept, squaric acid-based CMPs with simple preparation and abundant ion dipole interactions and hydrogen bonding for the reversible adsorption of gas molecules were selected as the desired platforms to hybridize NH_2-MWCNTs (**Scheme 1**) and investigated their chemiresistive gas sensing performance for the first time. In this work, a C—N cross-coupling technique was employed to synthesize various squaric acid-based CMPs with different ligands center, denoted as PSATA, PSATB, and PSATT, respectively. Among these, PSATT was further modified on the surface of NH_2-MWCNTs with varying amounts to obtain a series of conductivity-improved CMPs, denoted as PSATT-nNC (n = 3, 5, 7, 10). Furthermore, these CMPs were successfully applied in chemiresistive gas sensing to detect NO_2. Notably, the best of them, the response value of PSATT-7NC toward 4 ppm NO_2 is 9766% at 100 °C, which is 2.5 times higher than that of the pristine PSATT. These results demonstrate that the strategy of hybridizing NH_2-MWCNTs effectively enhances conductivity to achieve the improvement of sensing performance in CMPs. This work has successfully realized ultrasensitive NO_2 detection using CMPs-based materials, thereby paving the way for further exploration of amorphous POPs in gas sensing applications.

2. Results and Discussion

PSATA, PSATB, and PSATT were prepared through a simple and green substitution reaction of C—N cross-coupling method.[23] The synthetic route of these three squaric acid-based CMPs with different ligands center is shown in Figure S1a (Supporting Information). Among them, PSATT was further modified on the surface of NH_2-MWCNTs with varying amount to obtain PSATT-nNC (n = 3, 5, 7, 10) as depicted in the synthetic scheme shown in Figure S1b (Supporting Information) (details see the experiment section). The photos of the series of obtained CMP materials are shown in Figure S2 (Supporting Information). The morphologies of PSATA, PSATB, and PSATT were investigated through scanning electron microscopy (SEM) and transmission electron microscopy (TEM). SEM images show the morphologies of nanowires, nanoparticles, and nanorods as PSATA, PSATB, and PSATT, respectively (**Figure 1a-c**). TEM image showed that the nanorods of PSATT were ≈50 – 60 nm in diameter (Figure 1e). After modifying NH_2-MWCNTs, the morphologies of PSATT-nNC (n = 3, 5, 7, 10) showed that their surface is rougher than that of NH_2-MWCNTs with a uniform diameter of ≈37 nm (Figure 1d-i; Figures S3 and S4, Supporting Information). There is no big difference in the morphologies for PSATT-nNC (Figure S4, Supporting Information). However,

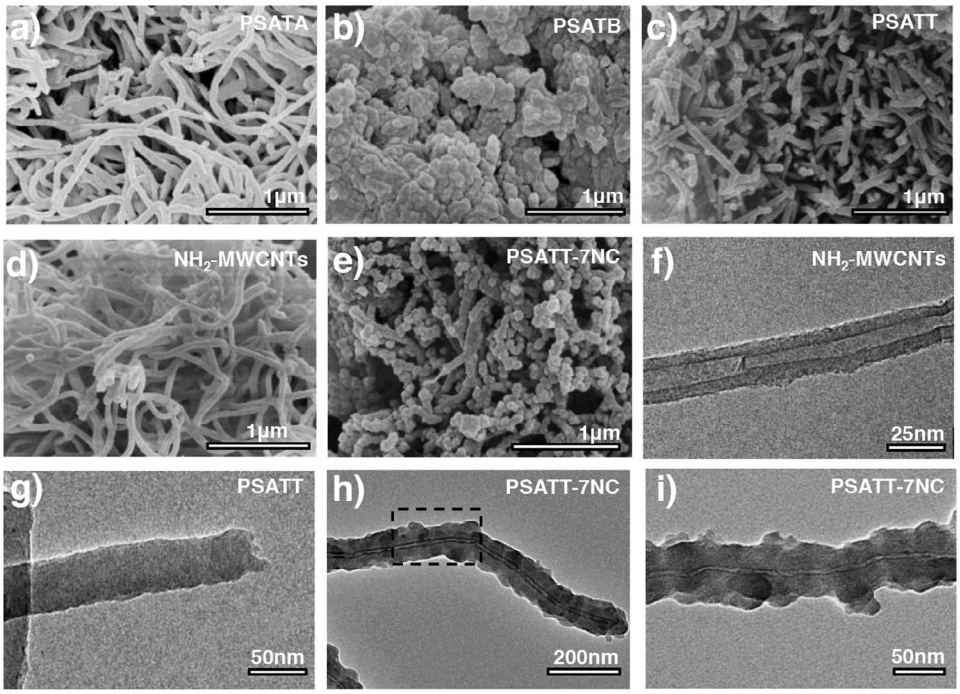

Figure 1. SEM images of a) PSATA, b) PSATB, c) PSATT, d) NH_2-MWCNTs and e) PSATT-7NC, TEM images of f) NH_2-MWCNTs, g) PSATT, and h–i) PSATT-7NC.

the diameter decreases as the amount of NH_2-MWCNTs from PSATT-3NC to PSATT-10NC, illustrating the reduction in the thickness of PSATT layer (Figure S4, Supporting Information). These results revealed that PSATT is successfully formed on the surface of NH_2-MWCNTs.

The detailed synthesis route of PSATA, PSATB and PSATT was displayed in **Figure 2**a. The chemical composition and structure of these CMP materials were characterized by Fourier-transform infrared (FT-IR), ^{13}C solid-state nuclear magnetic resonance (^{13}C NMR) spectra and ^{1}H solid-state nuclear magnetic resonance (^{1}H NMR) spectra. Concretely, the peak of near 1785 cm^{-1} for the characteristic vibration of the C═O bond and the peak of ≈1528 cm^{-1} corresponding to C—N—C bond were observed in the FT-IR spectra, which showed the presence of squaric acid units in the structure of PSATA, PSATB, PSATT and PSATT-nNC (n = 3, 5, 7, 10) (Figure 2b; Figures S8 and S9, Supporting Information). Furthermore, the new formation of C—N bond from the squaric acid linked to the amino monomer was evidenced by the appearance of signals at ≈140 ppm in the ^{13}C NMR spectra and 9.5 ppm in the ^{1}H NMR spectra, which clearly confirmed the successful synthesis of PSATA, PSATB, and PSATT (Figures S6 and S7, Supporting Information).

Powder X-ray diffraction (PXRD) showed that PSATA, PSATB and PSATT were amorphous polymers (Figure S10, Supporting Information). After hybridization with NH_2-MWCNTs, the PXRD peaks of PSATT-nNC nearly remained compared to pristine PSATT (Figure S10, Supporting Information). Moreover, the surface amino groups of NH_2-MWCNTs could provide the strong forces for hybridizing CMPs. Based on the same C—N cross-coupling reaction as PSATT synthesis, in PSATT-nNC, PSATT chemically bonds to the surface of NH_2-MWCNTs (Figure 2a). It was revealed by X-ray photoelectron spectroscopy (XPS) measurements of of PSATT and PSATT-nNC (Figures S11 and S12, Supporting Information). Through the semiquantitative analysis of XPS, the ratios of C—N and C—C in PSATT-nNC are significantly larger than that of pure PSATT to demonstrate the formation of more C—N bonds in PSATT-nNC (Figures S11 and S12, Supporting Information). These results confirmed the covalent bond between PSATT and the surface of NH_2-MWCNTs in PSATT-nNC.

The N_2 isothermal adsorption-desorption curves were measured at 77 K to reveal porous structures of these CMP materials. All samples showed the type-I isotherm, which demonstrated microporous structures (Figure 2f,g). The specific surface area (S_{BET}) of PSATA, PSATB, PSATT were 31.3, 68.6, and 78.6 $m^2\ g^{-1}$, respectively (Figure 2f,g; Table S1, Supporting Information). The increased in S_{BET} is attributed to the enhanced conjugation of these materials, which is brought about by the central regulation of the amino monomers (Figure 2a). After the modification of NH_2-MWCNTs, the S_{BET} of PSATT decreased and continued to decrease as the content of NH_2-MWCNTs increased (Figure 2f,g; Table S1, Supporting Information). Furthermore, the bandgap structures of PSATT, NH_2-MWCNTs, and PSATT-nNC were explored through UV–vis adsorption spectra and cyclic voltammetry (CV) measurements (Figure 2c; Figures S13 and S15, Supporting Information). With the enhancement of NH_2-MWCNTs amount from PSATT to PSATT-10NC, the bandgap gradually decreases (Figure S13, Supporting Information). As shown in Figure 2d; Figure S14 (Supporting Information), the valence bands/conduction bands for PSATT and PSATT-nNC (n = 3, 5, 7, 10) were further revealed from CV measurements.

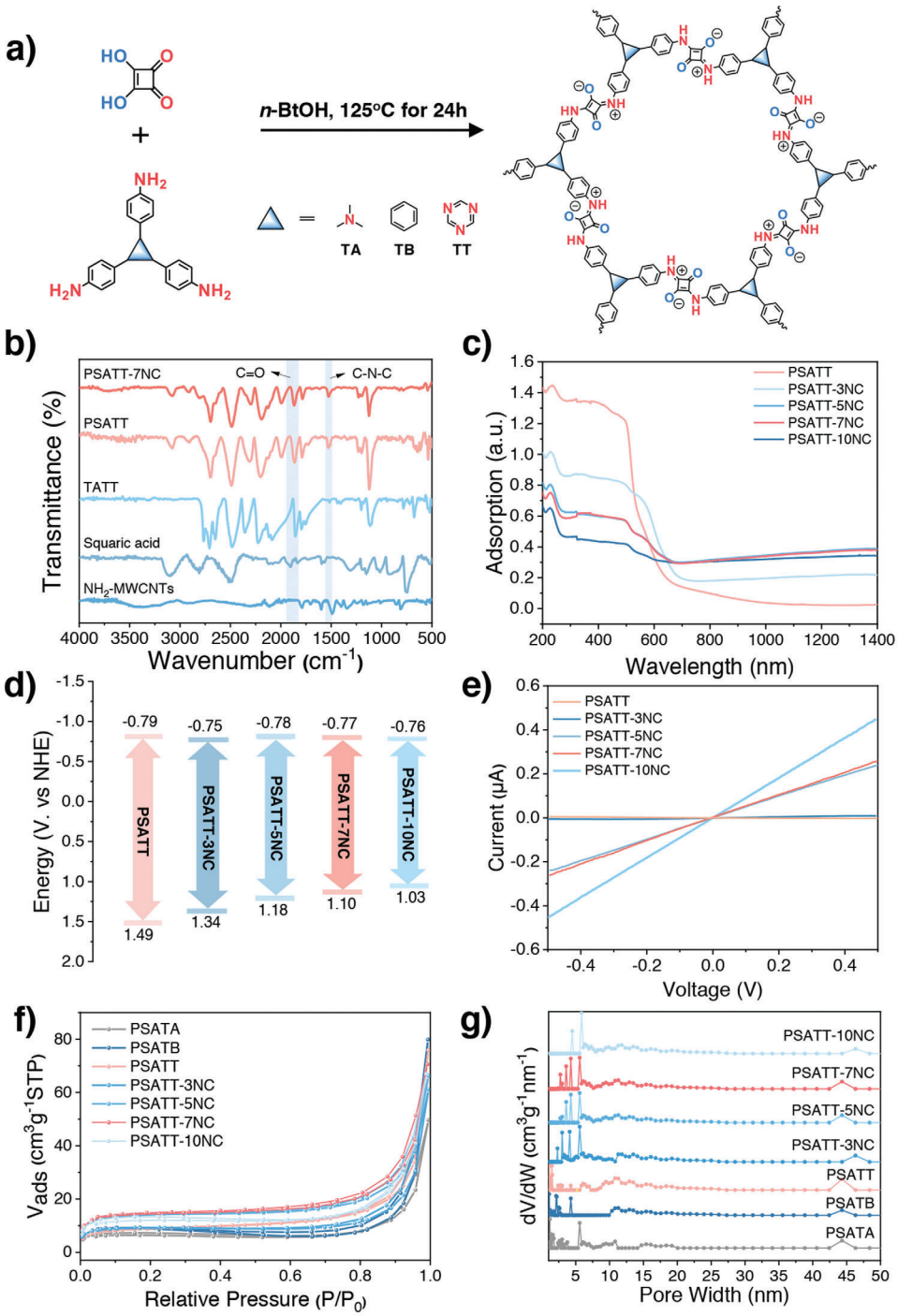

Figure 2. a) Synthetic route for the formation of PSATA, PSATB, and PSATT, b) FT-IR spectra of PSATT and PSATT-7NC, c) UV–vis absorption spectra of PSATT and PSATT-nNC (n = 3, 5, 7, 10) in the solid state, d) Energy band of PSATA, PSATB, PSATT, and PSATT-7NC, e) *I–V* curves of PSATT-nNC (n = 3, 5, 7, 10), f) N_2 adsorption and desorption isotherms (77 K), g) Density functional theory-pore size distribution of PSATA, PSATB, PSATT, and PSATT-nNC (n = 3, 5, 7, 10).

To prove that the conductivity of PSATT is improved after modification with NH_2-MWCNTs, we explored their electrical properties. The electrical conductions of PSATT and PSATT-nNC were measured through *I–V* curves (Figure 2e). Under room temperature, the conductivity gradually increases with the increase of NH_2-MWCNTs amount (Table S2, Supporting Information). The conductivity of PSATT-7NC and PSATT-10NC is ≈26 and 46.8 times higher than that of pristine PSATT (Table S2, Supporting Information). These results indicated that the NH_2-MWCNTs hybrid

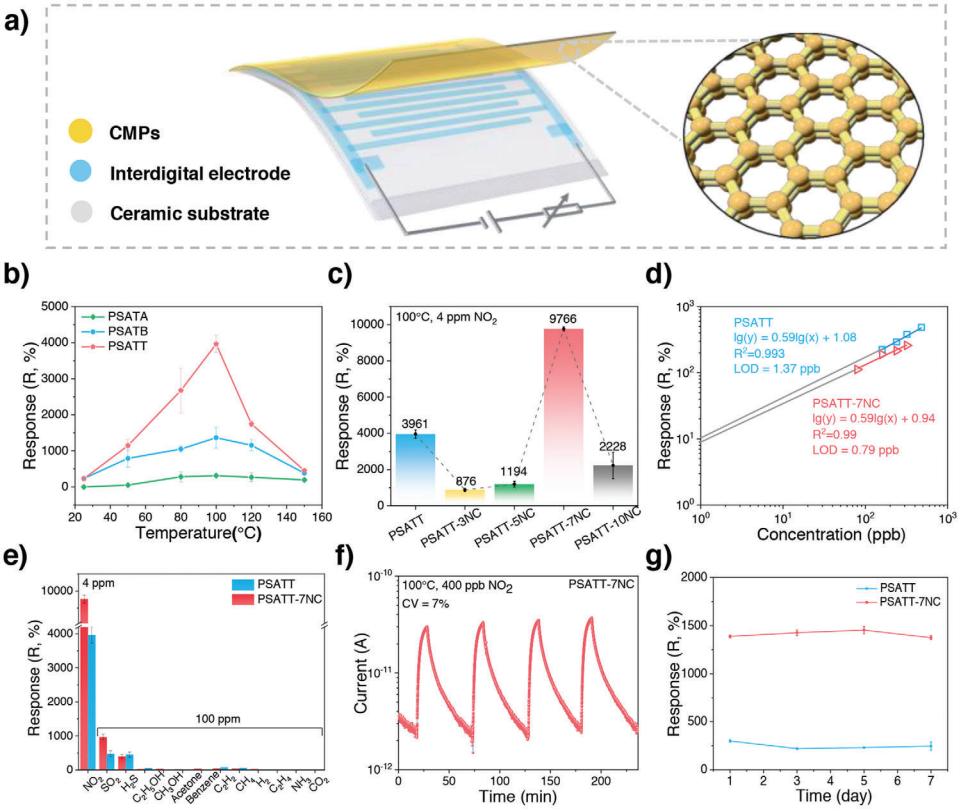

Figure 3. a) Schematic illustration of the sensing device, b) Temperature dependent response of PSATA, PSATB and PSATT toward 4 ppm NO_2, c) Column charts of response toward 4 ppm NO_2 of PSATT, PSATT-3NC, PSATT-5NC, PSATT-7NC and PSATT-10NC at 100 °C, d) Response-concentration log-log plots for PSATT and PSATT-7NC, e) Sensing response of PSATT and PSATT-7NC to various gases, f) Reproducibility of the PSATT-7NC-based sensors toward 0.4 ppm NO_2, g) Long-term stability of PSATT and PSATT-7NC toward 0.4 ppm NO_2.

strategy has successfully enhanced the conductivity of CMP materials.

The obtained series of CMPs with large surface area and improved conductivity might serve as desired platforms for chemiresistive gas sensing. These CMP materials were tested in a home-made system as shown in Figure S16 (Supporting Information) and the sensing devices were depicted in **Figure 3a**. To optimize the operating temperature of devices, the chemiresistive gas sensing of PSATA, PSATB and PSATT were tested within the temperature range of 25 to 150 °C toward 4 ppm NO_2 (Figure 3b; Figures S17 and S18, Supporting Information). All three samples reached its highest response value at 100 °C, indicating optimal working temperature of these devices. Under 100 °C and dark conditions, PSATT exhibited response value of 3961% toward 4 ppm NO_2, which is 12.7 times higher than PSATA and 3 times higher than PSATB (Figure 3b). Thereafter, the NO_2 sensing performance of PSATT-nNC is tested under the same conditions (Figure S19, Supporting Information). Compared with pristine PSATT, the response values of PSATT-3NC and PSATT-5NC are lower, which might be attributed to the reduction of S_{BET} (Figure 3c; Table S1, Supporting Information). However, as the amount of NH_2-MWCNTs increases, the response value of PSATT-nNC first increases and then decreases, reaching the maximum at PSATT-7NC, even exceeding pristine PSATT (Figure 3c). PSATT-7NC showed a response value of 9766%, which is 2.5 times higher than that of the pristine PSATT (Figure 3c). These results demonstrated that enhancing electrical conductivity effectively improves the sensing performance of CMP materials. With the introduction of NH_2-MWCNTs, the number of active sites decreases, leading to reduced sensing performance. However, as the amount of NH_2-MWCNTs increases, the resulting improvement in conductivity enhance the sensing properties. When the conductivity improvement is minor, it is insufficient to compensate for the performance reduction caused by the fewer active site, resulting in poor performance of PSATT-3NC and PSATT-5NC. When the level of modification reaches a critical threshold (PSATT-7NC), the conductivity enhancement compensates for the loss of active sites, yielding better performance than the original PSATT. However, further increasing the amount of NH_2-MWCNTs (PSATT-10NC) leads to a decline in sensing performance. This is because the conductivity of PSATT-7NC already fully meets the electron transport required for the material when it is applied to gas sensing. Therefore, the continuous increase in electrical conductivity (PSATT-10NC) does not significantly improve performance, but rather degrades performance due to the reduction of the active site. Additionally, PSATT and PSATT-7NC showed concentration-dependent response to NO_2 in the range of 0.16 to 4 ppm (Figure S20, Supporting Information). The theoretical limit of detections (LOD) for PSATT and PSATT-7NC were calculated to be ≈1.37 and 0.79 ppb,

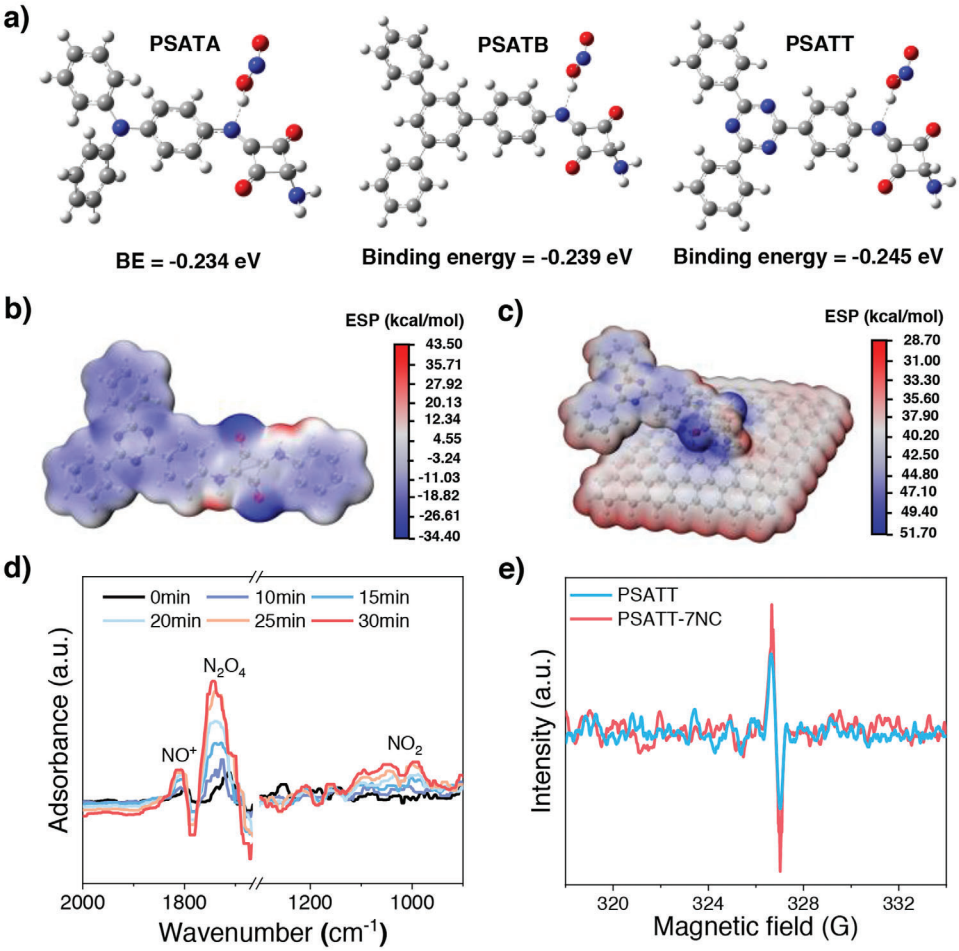

Figure 4. a) Calculated binding energy (BE) between CMPs and NO_2 at the optimum adsorption site, b,c) Electrostatic potential surface maps of PSATT and PSATT-7NC models, d) Time-resolved DRIFTS and e) EPR spectra of PSATT and PSATT-7NC.

respectively, by setting the response at 10% (Figure 3d). The LOD of PSATT-7NC is the lowest for all polymers-based sensors at low operating temperature (Table S3, Supporting Information).[25–29]

Selectivity is an important parameter for the sensing performance evaluation.[3,30–32] To explore gas sensing selectivity, PSATT and PSATT-7NC were conducted to exposure in 12 kinds of other interfering gases with a concentration of 100 ppm at 100 °C (Figure 3e; Figure S22, Supporting Information). Notably, the responses of PSATT and PSATT-7NC toward 4 ppm NO_2 were much higher than 100 ppm other interfering gases, indicating superior selectivity (Figure 3e; Figure S22, Supporting Information). In addition, the response/recovery time of PSATT and PSATT-7NC toward 4 ppm NO_2 at 100 °C are estimated to be 2.9/6.7 min and 2.9/13.9 min, respectively (Figure S19, Supporting Information).

Furthermore, the cycling stability of PSATT-7NC towards 4 ppm NO_2 was investigated (Figure 3f). PSATT-7NC-based sensors showed a low coefficient of variation (7%) over 4 cycles, indicating good repeatability (Figure 3f). The PSATT and PSATT-7NC are selected as the desirable platform for investigating the long-term stability. After 7 days, ≈90% of the original response value to 4 ppm NO_2 mixed air was retained, indicating excellent long-term stability of PSATT and PSATT-7NC (Figure 3g; Figure S23, Supporting Information).

The gas sensing mechanisms of PSATT and PSATT-7NC were systematically studied. First, possible adsorption sites of NO_2 molecules were investigated through density functional theory (DFT) calculation. Among all possible bonding models, the most stable interaction model formed the hydrogen bonds between two amide hydrogen atoms of PSATT and NO_2 molecules (**Figure** 4a). Compared to PSATA and PSATB, the O═N═O…H─N in PSATT exhibited the largest binding energy (0.245 eV), which matches the result of gas sensing test well.[33] Second, most charges of PSATT and PSATT-7NC were concentrated at the edge of molecules and exhibited a completely localized positive and negative charge distribution (Figure 4b,c). The results indicate that introduction of NH_2-MWCNTs did not significantly alter the charge distribution of CMPs to bring good electron transport. The energy level demonstrates that the electrons transfer from NH_2-MWCNTs to PASTT. The interaction between NO_2 and CMPs was investigated through the in situ diffuse reflectance infrared FT-IR spectroscopy (DRIFTs) to monitor the sensing process of PSATT when exposed to 4 ppm NO_2 (Figure 4d). It was

clearly showed the presence of adsorption peaks ascribed to oxygen vacancy (1807 cm^{-1}), NO_2 (1040 cm^{-1}) and N_2O_4 (1743 cm^{-1}) with the continuously increasing intensity under extending the exposure time.[23,34,35] Finally, both PSATT and PSATT-7NC exhibited different EPR signal intensity with g = 2.06 (Figure 4e), indicating the same type of EPR source with different amounts of cationic radical signals formed on nitrogen sites.[36,37] The formation of a cationic radical results in the generation of a free electron hole, which can facilitate high mobility within the conjugated structure when an external electric field is applied.[38] This increased mobility contributes to enhanced electrical conductivity in the materials. This improvement in electron transport results in superior sensing performance, with the sensitivity of PSATT-7NC reaching its maximum. Notably, the decline in sensing performance observed in PSATT-3NC and PSATT-5NC compared to pure PSATT can be attributed to the fact that the rise in conductivity resulting from the increase in free radicals is insufficient to offset the impact of the reduced surface area and the decline in active sites (Figure S24, Supporting Information).

3. Conclusion

In summary, three squaric acid-based CMPs were successfully synthesized and their chemiresistive gas sensing performance was investigated. Among them, PSATT exhibited the best performance and was selected as the desired platform to demonstrate the significance of enhancing conductivity through hybridization NH_2-MWCNTs in improving the chemiresistive gas sensing performance of CMP materials. As the amount of NH_2-MWCNTs increased, the electrical conductivity of PSATT gradually increased. Although the responses of PSATT-3NC, PSATT-5NC and PSATT-10NC are worse than PSATT,. PSATT-7NC exhibited an excellent response value of 9766%, which is 2.5 times higher than that of the pristine PSATT. PSATT-7NC also showed superior selectivity to NO_2, among 12 typical interference gases and excellent long-term stability for up to 7 days. This work provides a feasible strategy to design the high performance of CMP-based chemiresistive gas sensing materials.

Supporting Information

Supporting Information is available from the Wiley Online Library or from the author.

Acknowledgements

The authors gratefully acknowledge the financial support provided by the National Natural Science Foundation of China (52373172, 52073046, 52103106, 22325109, 22171263, 62227815 and 91961115), the National Key Research and Development Program of China (2022YFB3807100 and 2022YFB3807102), the Program of Shanghai Academic Research Leader (21XD1420200), the Chang Jiang Scholar Program (T2023082), the Natural Science Foundation of Shanghai (23ZR1401100), Scientific Research and Equipment Development Project of CAS (YJKYQ20210024), the China Postdoctoral Science Foundation (2023M743496), the Postdoctoral Fellowship Program of CPSF under Grant Number GZC20241722 and the State Key Laboratory for Modification of Chemical Fibers and Polymer Materials (KF2408).

Conflict of Interest

The authors declare no conflict of interest.

Data Availability Statement

The data that support the findings of this study are available in the supplementary material of this article.

Keywords

conjugated microporous polymers, gas sensing, NH_2-MWCNTs composites, NO_2 detection

Received: September 3, 2024
Revised: November 29, 2024
Published online:

[1] X. Zhou, S. Lee, Z. Xu, J. Yoon, *Chem. Rev.* **2015**, *115*, 7944.
[2] H. Wang, W. P. Lustig, J. Li, *Chem. Soc. Rev.* **2018**, *47*, 4729.
[3] R. A. Potyrailo, *Chem. Rev.* **2016**, *116*, 11877.
[4] Y. Zhang, Y. Wang, C. Gao, Z. Ni, X. Zhang, W. Hu, H. Dong, *Chem. Soc. Rev.* **2023**, *52*, 1331.
[5] X. Liu, W. Zheng, R. Kumar, M. Kumar, J. Zhang, *Coord. Chem. Rev.* **2022**, *462*, 214517.
[6] Y. Jian, W. Hu, Z. Zhao, P. Cheng, H. Haick, M. Yao, W. Wu, *Nano-Micro Lett.* **2020**, *12*, 71.
[7] Y. M. Jo, Y. K. Jo, J. H. Lee, H. W. Jang, I. S. Hwang, D. J. Yoo, *Adv. Mater.* **2023**, *35*, 2206842.
[8] R. Kumar, X. Liu, J. Zhang, M. Kumar, *Nano-Micro Lett.* **2020**, *12*, 164.
[9] L. X. Ou, M. Y. Liu, L. Y. Zhu, D. W. Zhang, H. L. Lu, *Nano-Micro Lett.* **2022**, *14*, 206.
[10] S. Wang, H. Li, H. Huang, X. Cao, X. Chen, D. Cao, *Chem. Soc. Rev.* **2022**, *51*, 2031.
[11] L. Zou, Y. Sun, S. Che, X. Yang, X. Wang, M. Bosch, Q. Wang, H. Li, M. Smith, S. Yuan, Z. Perry, H. C. Zhou, *Adv. Mater.* **2017**, *29*, 1700229.
[12] Y. Zhu, P. Xu, X. Zhang, D. Wu, *Chem. Soc. Rev.* **2022**, *51*, 1377.
[13] Z. Chen, K. O. Kirlikovali, K. B. Idrees, M. C. Wasson, O. K. Farha, *Chem* **2022**, *8*, 693.
[14] X. Liu, C. F. Liu, S. Xu, T. Cheng, S. Wang, W. Y. Lai, W. Huang, *Chem. Soc. Rev.* **2022**, *51*, 3181.
[15] Z. Li, Y. W. Yang, *Adv. Mater.* **2022**, *34*, 2107401.
[16] W. He, J. Duan, H. Liu, C. Qian, M. Zhu, W. Zhang, Y. Liao, *Prog. Polym. Sci.* **2024**, *148*, 101770.
[17] N. Meng, Y. Zhang, W. Liu, Q. Chen, N. Soykeabkaew, Y. Liao, *Adv. Funct. Mater.* **2024**, *34*, 2313534.
[18] J.-S. M. Lee, A. I. Cooper, *Chem. Rev.* **2020**, *120*, 2171.
[19] X. Liu, Y. Xu, D. Jiang, *J. Am. Chem. Soc.* **2012**, *134*, 8738.
[20] H. Ben, G. Yan, H. Liu, C. Ling, Y. Fan, X. Zhang, *Adv. Funct. Mater.* **2022**, *32*, 2104519.
[21] C. Yu, J. H. He, X. F. Cheng, H. Z. Lin, H. Yu, J. M. Lu, *Angew. Chem., Int. Ed.* **2021**, *60*, 15328.
[22] H. Roh, D. H. Kim, Y. Cho, Y. M. Jo, J. A. del Alamo, H. J. Kulik, M. Dincă, A. Gumyusenge, *Adv. Mater.* **2024**, *36*, 2312382.
[23] C. Yu, H. Z. Lin, J. Zhou, X. F. Cheng, J. H. He, H. Li, Q. F. Xu, N. J. Li, D. Y. Chen, J. M. Lu, *J. Mater. Chem. A* **2020**, *8*, 1052.
[24] J. Wang, Q. Cao, X. F. Cheng, W. Ye, J. H. He, J. M. Lu, *ACS Sens.* **2022**, *7*, 3782.
[25] H. Park, D. H. Kim, B. S. Ma, E. Shin, Y. Kim, T. S. Kim, F. S. Kim, I. D. Kim, B. J. Kim, *Adv. Sci.* **2022**, *9*, 2200270.
[26] O. Moncea, J. Casanova-Chafer, D. Poinsot, L. Ochmann, C. D. Mboyi, H. O. Nasrallah, E. Llobet, I. Makni, M. El Atrous, S.

Brandès, Y. Rousselin, B. Domenichini, N. Nuns, A. A. Fokin, P. R. Schreiner, J. C. Hierso, *Angew. Chem., Int. Ed.* **2019**, *58*, 9933.
[27] Y. Shen, G. Li, S. Zhao, J. Bai, Z. Liu, B. Cui, D. Wei, D. Meng, F. Meng, *Sens. Actuators, B* **2023**, *388*, 133804.
[28] Y. J. Chen, M. Liu, J. Chen, X. Huang, Q. H. Li, X. L. Ye, G. E. Wang, G. Xu, *Chem. Sci.* **2023**, *14*, 4824.
[29] M. Liu, Y. J. Chen, X. Huang, L. Z. Dong, M. Lu, C. Guo, D. Yuan, Y. Chen, G. Xu, S. L. Li, Y. Q. Lan, *Angew. Chem., Int. Ed.* **2022**, *61*, e202115308.
[30] G. Lei, H. Pan, H. Mei, X. Liu, G. Lu, C. Lou, Z. Li, J. Zhang, *Chem. Soc. Rev.* **2022**, *51*, 7260.
[31] H. Y. Li, S. N. Zhao, S. Q. Zang, J. Li, *Chem. Soc. Rev.* **2020**, *49*, 6364.
[32] L. Pirondini, E. Dalcanale, *Chem. Soc. Rev.* **2007**, *36*, 695.
[33] S. Enoch, A. B. Nipate, V. Lakshmi, R. R. Malakalapalli, *Chem. Commun.* **2023**, *59*, 8846.
[34] A. Mahmood, X. Wang, X. Xie, J. Sun, *Colloids Surf. A* **2021**, *626*, 127058.
[35] W. Ye, L. Zhao, H. Z. Lin, L. Ding, Q. Cao, Z. K. Chen, J. Wang, Q. M. Sun, J. H. He, J. M. Lu, *Nat. Commun.* **2023**, *14*, 2133.
[36] Y. Yue, H. Li, H. Chen, N. Huang, *J. Am. Chem. Soc.* **2022**, *144*, 2873.
[37] Y. Xiong, Z. Wang, Y. Li, Y. Chen, L. Dong, *J. Am. Chem. Soc.* **2024**, *146*, 22777.
[38] P. P. Power, *Chem. Rev.* **2003**, *103*, 789.